



Characteristics of Copper-based Oxygen Carriers Supported on Calcium Aluminates for Chemical-Looping Combustion with Oxygen Uncoupling (CLOU)

Felix Donat,^{*,†} Wenting Hu,[†] Stuart A. Scott,[‡] and John S. Dennis[†]

[†]Department of Chemical Engineering and Biotechnology, University of Cambridge, Pembroke Street, Cambridge CB2 3RA, United Kingdom

[‡]Department of Engineering, University of Cambridge, Trumpington Street, Cambridge CB2 1PZ, United Kingdom

ABSTRACT: Eight different oxygen carriers (OC) containing CuO (60 wt %) and different mass ratios of CaO to Al₂O₃ as the support were synthesized by wet-mixing followed by calcination at 1000 °C. The method of synthesis used involved the formation of calcium aluminum hydrate phases and ensured homogeneous mixing of the Ca²⁺ and Al³⁺ ions in the support at the molecular level. The performance of the OCs for up to 100 cycles of reduction and oxidation was evaluated in both a thermogravimetric analyzer (TGA) and a fluidized bed reactor, covering a temperature range of 800 to 950 °C. In these cycling experiments, complete conversion of the OC, from CuO to Cu and vice versa, was always achieved for all OCs. The reactivity of the materials was so high that no deactivation could be observed in the TGA, owing to mass transfer limitations. It was found that OCs prepared with a mass ratio of CaO to Al₂O₃ in the support >0.55 agglomerated in the fluidized bed, resulting in an apparent deactivation over 25 cycles for all temperatures investigated. High ratios of mass of CaO to Al₂O₃ in the support resulted in CuO interacting with CaO, forming mixed oxides that have low melting temperatures, and this explains the tendency of these materials to agglomerate. This behavior was not observed when the mass ratio of CaO to Al₂O₃ in the support was ≤0.55 and such materials showed excellent cyclic stability operating under redox conditions at temperatures as high as 950 °C.

1. INTRODUCTION

In the chemical looping combustion (CLC) of solid fuels, achieving a sufficiently high rate of gasification of the char to synthesis gases in the fuel reactor is often difficult.^{1–3} However, at typical operating temperatures (~900 °C) some metal oxides, e.g., those containing Cu(II) or Mn(III), decompose to a lower metal oxide with the production of gas-phase oxygen. Accordingly, these materials are of interest for chemical looping with oxygen uncoupling (CLOU), a variant of CLC in which the char is largely oxidized by the gaseous oxygen released by certain oxygen carriers (OC), rather than being gasified to synthesis gas, which in turn reduces the OC.¹

Leion et al.² showed that, compared to conventional CLC, the overall rate of conversion of, e.g., petroleum coke to products of combustion was enhanced in CLOU (with a CuO-based OC) by a factor of ~80. For a given rate of fuel feeding, the faster rate of conversion of the fuel means that the total solids inventory and the total reactor volume can also be reduced, saving capital costs. From the combined effects of the faster kinetics and the higher oxygen capacity, Eyring et al.³ calculated the required mass loading of the active metal in the OC per MW_{th} fuel input to be ~135 kg with CuO, compared to ~1200 kg using Fe₂O₃-based OCs in conventional CLC.

Circulating fluidized bed (CFB) reactors would probably be used for CLC at large scale, i.e., several hundred MW_{th}.^{4,5} The OC particles in such reactors would undergo significant mechanical stress, and the priority should therefore be to improve their mechanical stability,⁶ to minimize losses by attrition and particle breakup. This is especially important where CLOU is to be used, because the oxides suitable for

CLOU, e.g., CuO, are more costly than those used in conventional CLC, e.g., iron oxide, possibly by a factor of ~10.⁷

For CLOU materials, such as CuO, calcium aluminate cement has been shown to be a promising support, stabilizing the resulting OC both chemically and mechanically.^{8–10} This paper is concerned with the manufacture of such oxygen carriers, with CuO supported on calcium aluminates. The objective was to produce durable OC particles with a high oxygen transfer capacity using low-cost, environmentally benign precursors, viz. CaO and Al₂O₃. The main difficulty in producing such particles lies in preventing any interaction of the CaO and the Al₂O₃ with the CuO. For example, for the case of CuO and Al₂O₃, CuAl₂O₄ could form, lowering the effective amount of oxygen available for CLOU, because the release of oxygen from the aluminate does not proceed at an appreciable rate.^{11,12} Indeed, Song et al.¹³ and Imtiaz et al.¹⁴ suggested that the interaction of the CuO with Al₂O₃ could be prevented by the presence of Na-containing contaminants that render the Al₂O₃ inactive, possibly via the formation of inert NaAlO₂. Given the thermodynamic stability of calcium aluminates, a similar effect would be expected with additions of CaO. However, there is also the potential for a reaction between CuO and CaO at temperatures below 1000 °C.¹⁵ The resulting mixed oxides have rather low melting temperatures and can potentially cause agglomeration in a fluidized bed.

Received: March 29, 2015

Revised: June 11, 2015

Accepted: June 15, 2015

Published: June 15, 2015

Table 1. Comparison and Properties of the 60 wt % CuO Oxygen Carrier Particles as Prepared

batch number	1	2	3	4	5	6	7	8
ratio of CaO to Al ₂ O ₃ in the support (g/g)	0.09	0.22	0.28	0.39	0.55	0.72	0.94	1.65
bulk density (kg/m ³)	567	744	715	734	825	1615	1616	1892
calcium aluminate phases identified by XRD	CaAl ₄ O ₇	CaAl ₄ O ₇ CaAl ₂ O ₄	CaAl ₄ O ₇ CaAl ₂ O ₄	CaAl ₂ O ₄ CaAl ₄ O ₇	Ca ₁₂ Al ₁₄ O ₃₃ CaAl ₂ O ₄	Ca ₁₂ Al ₁₄ O ₃₃ CaAl ₂ O ₄	Ca ₁₂ Al ₁₄ O ₃₃	Ca ₁₂ Al ₁₄ O ₃₃ Ca ₃ Al ₂ O ₆
copper phases identified by XRD	CuO, CuAl ₂ O ₄	CuO, CuAl ₂ O ₄	CuO, (CuAl ₂ O ₄)	CuO, (CuAl ₂ O ₄)	CuO	CuO	CuO	CuO, Ca ₃ Cu ₇ O ₁₀

Calcium aluminates can be made by mixing powdered CaO and Al₂O₃ at high temperature (>1400 °C) during which they become molten as the product forms.¹⁶ However, the resulting calcium aluminate cannot be used immediately as a support material in an OC because it has to be finely ground and the resulting powder mixed with the CuO. Contact with water makes the calcium aluminate set rapidly, so that techniques for the preparation of particles, such as granulation, extrusion and spheronization, are not easily applied.

The production of calcium aluminates as support material in a CuO-based OC at a low temperature requires the Ca- and Al-precursors to the aluminates to be mixed on a microscopic, perhaps atomic, scale, so that upon calcination the calcium aluminate phase readily forms, without free Al₂O₃ or CaO that could interact with the CuO. Hydrothermal synthesis has been used to produce various calcium aluminate precursor species, such as Ca₃[Al(OH)₆]₂ or the cementitious compound Ca₄Al₂O₆(CO₃)11H₂O, a so-called layered double-hydroxide (LDH).^{17,18} In fact, Sauman and Lach¹⁹ found that Ca₄Al₂O₆(CO₃)11H₂O forms via the carbonation of Ca₃[Al(OH)₆]₂; both phases can normally be found in Portland cement or calcium aluminate cements, as hydration products of Ca₃Al₂O₆.¹⁶ Other products of the hydration of calcium aluminates include multiple metastable phases that eventually transform into Ca₃[Al(OH)₆]₂ as the only stable phase.^{16,20–22}

Ca–Al LDHs, such as calcium monocarboaluminate hydrate, Ca₄Al₂O₆(CO₃)11H₂O, have been successfully synthesized for molar ratios Ca²⁺/Al³⁺ ranging from 1 to 3, with CO₃²⁻ as the interlayer anion.^{17,18,23–25} The limitation on the Ca²⁺/Al³⁺ at which Ca–Al LDH can form means that of the various calcium aluminate phases formed on calcination (CaAl₁₂O₁₉, CaAl₄O₇, CaAl₂O₄, Ca₁₂Al₁₄O₃₃ and Ca₃Al₂O₆), only Ca₃Al₂O₆ can be synthesized via an LDH precursor. In this work, CuO-based oxygen carriers with calcium aluminate supports, produced by a low temperature (and readily scalable) wet mixing method are investigated. Powdered precursors were used, Ca(OH)₂ and Al(OH)₃, for the calcium aluminate phase and CuO as the active phase. Eight different oxygen carriers were made, consisting of 60 wt % CuO and 40 wt % of a calcium aluminate support, covering the entire spectrum of the calcium aluminate phases,²⁶ including those that could form an LDH precursor. Accordingly, any advantages such as structuring in the final mixed oxides, offered by producing the OCs via the LDH phase could be ascertained. The materials were characterized by powder X-ray diffraction (XRD) analysis and scanning electron microscopy (SEM). Two sets of experiments were carried out at constant temperatures and atmospheric pressure to evaluate the performance of these materials: (i) reactivity tests in a thermogravimetric analyzer for up to 100 cycles of reduction and oxidation, and (ii) investigation of the cyclic stability of the OCs in a fluidized bed reactor (FBR) at temperatures between 800 and 950 °C, where also resistance to attrition and agglomeration is important.

2. EXPERIMENTAL SECTION

2.1. Synthesis of the Oxygen Carrier. The oxygen carriers investigated in this study consisted of 60 wt % CuO and 40 wt % of a calcium aluminate support. Eight different oxygen carriers with different compositions of the support were synthesized as follows. For a batch size of ~50 g of OC, powders of Al(OH)₃ (Sigma-Aldrich, <5 μm, reagent grade) and Ca(OH)₂ (Acros Organics, <5 μm, 98 wt %) were mixed with ~400 mL of deionized water and stirred on a magnetic hot plate at ~40 °C for 2 h, open to the atmosphere. The CO₃²⁻ ions required for the formation of the Ca–Al LDH were provided by the dissolution of atmospheric CO₂ in the limewater formed by the sparingly soluble calcium hydroxide.^{21,27,28} The pH of the alkaline suspension was ~12.3, so that only CO₃²⁻ ions would have formed.²⁷ Gaseous CO₂ from the cylinder was not used, as this would have resulted in a much lower pH and also the formation of HCO₃⁻ ions, making the hydration reactions more complex and potentially reducing the repeatability of the synthesis process. Subsequently, CuO powder (Sigma-Aldrich, <10 μm, 98 wt %) was added and the suspension was stirred for another ~24 h, until the volume had significantly reduced and a viscous calcium aluminate gel had formed. The gel was a hydration product of Ca(OH)₂ and Al(OH)₃ and prevented the (heavier) CuO powder from settling, thus ensuring a homogeneous suspension.^{21,29} The extent of the formation of the gel was found to depend on the ratio of Ca(OH)₂ to Al(OH)₃, but was only noticeable once excess water had been removed by evaporation. No significant difference was observed when the temperature was varied from ~20 to 60 °C.

After drying for ~48 h at 80 °C in an oven, the mixture was crushed, sieved to 300–850 μm and the resulting green particles were calcined at 1000 °C for 6 h. The sieve fraction 355–425 μm was used in each experiment. The properties of all OCs are summarized in Table 1. For clarity, the content of Ca- and Al-species in each batch is expressed as the mass ratio of the corresponding oxides, i.e., CaO and Al₂O₃. XRD analysis, using a PANalytical Empyrean multipurpose diffractometer, was undertaken on all eight OCs after calcination, with the phases detected shown in Table 1. The formation of these phases is discussed in detail, in Sections 3 and 4.

2.2. Apparatus. Two different experimental reactors were used: a thermogravimetric analyzer (TGA), (Mettler Toledo TGA/DSC 1 STARE system), and a fluidized bed reactor (FBR), operating in batch mode, described below.

TGA. The oxygen carrier materials were initially investigated in the TGA, to evaluate their chemical stability at 900 °C. The sample chamber of the TGA was purged throughout the experiments with N₂ at a flow rate of 50 mL/min (as measured at 20 °C and 1 atm). Additionally, a protective gas (N₂, 50 mL/s at 20 °C and 1 atm) was passed through the balance. The samples (~20 mg) were placed in a 70 μL alumina crucible and reduced and oxidized repeatedly by the reactant gases at a flow

rate of ~ 100 mL/min (at 20 °C and 1 atm). First, the OC was exposed to N_2 for 600 s, followed by the reduction using 5 mol % H_2 (balance N_2) for another 600 s. Finally, the OC was reoxidized using air for 600 s. Between 25 and 100 cycles of reduction and oxidation were performed for each OC.

The conversion, X , of the OC at time t was defined as

$$X = \frac{m_t - m_{\text{reduced}}}{m_{\text{oxidized}} - m_{\text{reduced}}} \quad (1)$$

where m_t was the mass of the sample at time t , m_{reduced} was the mass when the OC was reduced fully, i.e., to Cu, and m_{oxidized} was the mass when the OC was in its fully oxidized state, i.e., as CuO. The observed oxygen capacities for the reduction of CuO to Cu_2O , R_{OC,Cu_2O} , and CuO to Cu, $R_{OC,Cu}$, respectively, were defined as

$$R_{OC,Cu_2O} = \frac{m_{\text{reduced},N_2} - m_{\text{reduced,exp}}}{m_{\text{oxidized,exp}}} \quad (2)$$

and

$$R_{OC,Cu} = \frac{m_{\text{oxidized,exp}} - m_{\text{reduced,exp}}}{m_{\text{oxidized,exp}}} \quad (3)$$

where m_{reduced,N_2} denotes the mass of the sample after the OC had decomposed from CuO to Cu_2O ; $m_{\text{reduced,exp}}$ and $m_{\text{oxidized,exp}}$ correspond, respectively, to the mass measured at the end of the reduction and oxidation periods in a cycle.

Fluidized Bed Reactor. The fluidized bed reactor (FBR) used to perform cycles of oxidation and reduction is shown schematically in Figure 1. The reaction vessel consisted of an

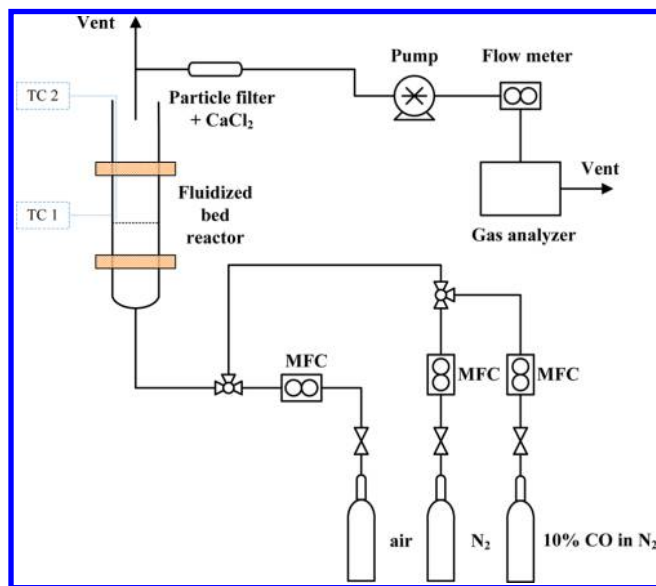


Figure 1. Schematic diagram of the experimental apparatus using the fluidized bed reactor.

electrically heated tube (Incoloy 800 HT, i.d. of 16 mm) with a heated section of length ~ 140 mm between two water cooled copper electrodes; current was supplied via a transformer (2.5 V, 1600 A) allowing heating rates of ~ 400 °C/min. The heated section was insulated (Superwool 607 Max Blanket) to minimize heat losses. About 15 mm below the middle of the heated section, a sintered quartz distributor (porosity grade 1) was fitted on a stainless steel support to act as the distributor.

The pressure drop across the distributor was ~ 1300 Pa, ensuring uniform fluidization of the bed.³⁰ Below the distributor, a plug of quartz wool was placed to aid mixing of the gas.

The FBR could be fluidized with mixtures of N_2 , air and CO (10 mol % in N_2), depending on the desired reaction conditions. Hydrogen was not used as the reducing gas in these experiments because the oxidation product, H_2O , could not be measured accurately. Neither the type of fuel gas, nor the concentration was varied, as measuring the intrinsic kinetics of the materials was not the primary objective of this work. All gases were provided by BOC Ltd. from cylinders. Gas flows were controlled by three calibrated mass flow controllers (Bronkhorst, EL-Flow series).

A fraction of the exhaust gas from the fluidized bed was continuously sampled by a diaphragm pump (at ~ 0.5 l/min, measured at 20 °C and 1 atm) through a 6.25 mm o.d. tube inserted from above, ~ 50 mm into the reaction vessel, while most of the exhaust gas was vented to the laboratory extraction system. The sampled gas passed through a particle filter and a water vapor trap ($CaCl_2$) to remove any moisture. An ABB EL3020 gas analyzer was used to analyze (at a frequency of 1 Hz) the gas flow for concentrations of CO, CO_2 (nondispersive infrared analyzer) and O_2 (paramagnetic analyzer).

The FBR was used to evaluate the cyclic performance of the OCs while fluidized in the bubbling regime over 25 redox cycles at 800, 850, 900 and 950 °C. The bed consisted of ~ 5 g of silica sand (sieved to 425–500 μm) as an inert material and ~ 0.4 g of OC. The silica sand acted as a temperature buffer to maintain a relatively constant bed temperature during the exothermic reduction and oxidation reactions. Despite the dilution with silica sand, the amount of OC used in an experiment was sufficient so that their tendency toward agglomeration could be studied. Under the conditions investigated, any chemical interaction of the silica sand with the OC materials was not expected nor observed. The total height of the bed in the reactor was ~ 18 mm (unfluidized), ensuring a uniform bed temperature profile under operating conditions, measured using a K-type thermocouple. The inlet gas flow rate was kept constant at 20 mL/s (as measured at 20 °C and 1 atm), such that the ratio of superficial gas velocity to that required for fluidization, U_0/U_{mf} varied with temperature from ~ 7 to 9 (calculated for the sand with a shape factor of 0.83, based on the Ergun equation for small particles, as described by Kunii and Levenspiel³¹). Each cycle consisted of four periods: (1) N_2 for 300 s from t_0 to t_1 , (2) 10 mol % CO in N_2 for 300 s from t_1 to t_2 , (3) N_2 for 60 s from t_2 to t_3 and (4) air for 300 s from t_3 to t_4 (diluted with N_2 by a factor of 2 at 950 °C, or a factor of 4 below 950 °C, to limit the temperature rise of the bed due to the strongly exothermic oxidation reaction and to keep the thermodynamic driving force for the oxidation reaction roughly the same at all temperatures). Before OC was added to the bed, blank runs were performed to account for any unwanted side reactions of the reactor material with the reducing and oxidizing gases. The ultimate conversions of the OC achieved during the different stages of reaction were calculated from the measured off-gas concentrations, $x_{i,out}$:

$$X_{\text{red,CuO-Cu}_2\text{O}} = \frac{2 \cdot M_{\text{CuO}} \cdot \dot{n}_{\text{tot,in}}}{m_{\text{OC}} \cdot a_{\text{OC}}} \int_{t_0}^{t_1} \frac{x_{\text{O}_2,\text{out}}}{1 - x_{\text{O}_2,\text{out}}} \cdot dt \quad (4)$$

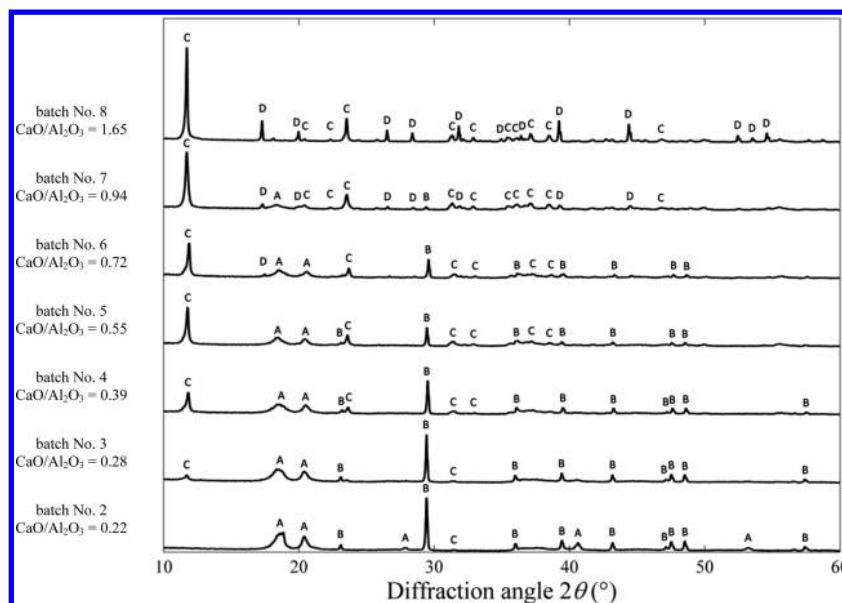


Figure 2. X-ray diffraction patterns of seven batches (2–8), prepared without CuO, before calcination. The peaks corresponding to crystalline phases were labeled as (A) $\text{Al}(\text{OH})_3$, (B) CaCO_3 , (C) $\text{Ca}_4\text{Al}_2\text{O}_6(\text{CO}_3)_{11}\text{H}_2\text{O}$ and (D) $\text{Ca}_3[\text{Al}(\text{OH})_6]_2$.

$$X_{\text{red,CuO-Cu}} = \frac{M_{\text{CuO}} \cdot \dot{n}_{\text{tot,in}}}{m_{\text{OC}} \cdot a_{\text{OC}}} \int_{t_1}^{t_2} x_{\text{CO}_2,\text{out}} \cdot dt \quad (5)$$

$$X_{\text{ox}} = \frac{2 \cdot M_{\text{CuO}} \cdot \dot{n}_{\text{tot,in}}}{m_{\text{OC}} \cdot a_{\text{OC}}} \int_{t_3}^{t_4} \frac{x_{\text{O}_2,\text{in}} - x_{\text{O}_2,\text{out}}}{1 - x_{\text{O}_2,\text{out}}} \cdot dt \quad (6)$$

In eqs 4–6, m_{OC} is the mass of the OC (g), a_{OC} is the mass fraction of the copper oxide in the OC and equal to 0.6, $\dot{n}_{\text{tot,in}}$ is the total number of moles entering the reactor in the gas-phase (mol/s) and M_{CuO} is the molecular weight of CuO (g/mol). Also, $x_{i,\text{in}}$ and $x_{i,\text{out}}$ denote, respectively, the concentrations of gas i entering and leaving the reactor. Where the conversion is plotted as a function of time, eqs 4–6 are used but the upper limit of the integral is adjusted accordingly.

For the definition of the conversion given in eq 4 for the period of oxygen release, the conversion of the OC will range from 0 (as CuO) to 0.5 (as Cu_2O). The overall conversion between t_0 and t_2 , i.e., the amount of oxygen removed from the oxygen carrier over both the oxygen release period and the reduction period compared to the total oxygen available, is given by $X_{\text{red,CuO-Cu}_2\text{O}} + X_{\text{red,CuO-Cu}}$.

3. RESULTS

3.1. Characterization of the Ca–Al Precursor, Before Calcination. The OCs were investigated after they had been dried at 80 °C, both by XRD (PANalytical Empyrean multipurpose diffractometer) and SEM (Zeiss EVO LS15). The materials had been prepared both with and without the CuO. The diffraction peaks for the CuO were dominant and there was no indication that the CuO had reacted with the $\text{Ca}(\text{OH})_2$ or the $\text{Al}(\text{OH})_3$ before calcination. For the purpose of clarity, only the XRD pattern for the materials prepared without the CuO is discussed in this section, because the additional CuO peaks of high intensity make identifying the smaller diffraction peaks of lower intensity more difficult.

The diffraction patterns for the Ca–Al supports, representing batches 2–8, are shown in Figure 2. For the highest mass ratio of CaO to Al_2O_3 = 1.65 (corresponding to molar ratio $\text{Ca}^{2+}/$

Al^{3+} = 1.5), the two main diffraction peaks appeared at $2\theta = 11.7$ and 23.5° , characteristic of an LDH structure identified as calcium monocarboaluminate hydrate, $\text{Ca}_4\text{Al}_2\text{O}_6(\text{CO}_3)_{11}\text{H}_2\text{O}$.^{16–18,32} The same LDH peaks can be seen for batches 3–7, with decreasing intensity for lower $\text{CaO}/\text{Al}_2\text{O}_3$; analogously, the peaks for $\text{Al}(\text{OH})_3$ and CaCO_3 become more dominant, indicating that for low $\text{CaO}/\text{Al}_2\text{O}_3$, less of the initial $\text{Ca}(\text{OH})_2$ and $\text{Al}(\text{OH})_3$ combined under the given reaction conditions. The peaks for CaCO_3 are due to the carbonation of $\text{Ca}(\text{OH})_2$ with atmospheric CO_2 and in the dried samples no crystalline $\text{Ca}(\text{OH})_2$ was detected. Additional peaks for batch 8 were identified as $\text{Ca}_3[\text{Al}(\text{OH})_6]_2$, the stable phase resulting from the hydration of calcium aluminates, and were also seen in batches 6 and 7.

The evolution of the plate-like LDH structure was further confirmed by SEM, Figure 3. The morphology of batch 2

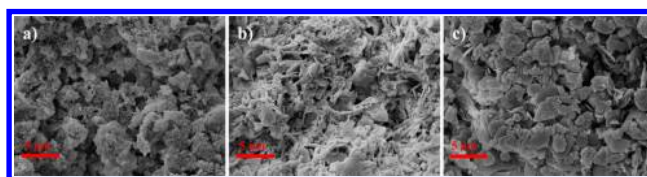


Figure 3. Scanning electron microscope images at a magnification of 10000 \times , before calcination. (a) Batch 2 ($\text{CaO}/\text{Al}_2\text{O}_3 = 0.22$), (b) batch 5 ($\text{CaO}/\text{Al}_2\text{O}_3 = 0.55$) and (c) batch 8 ($\text{CaO}/\text{Al}_2\text{O}_3 = 1.65$). The materials were prepared without CuO.

($\text{CaO}/\text{Al}_2\text{O}_3 = 0.22$) shows very little order, whereas batch 5 ($\text{CaO}/\text{Al}_2\text{O}_3 = 0.55$) contains some branched plate-like constructs, potentially stabilizing the material mechanically. Batch 8 ($\text{CaO}/\text{Al}_2\text{O}_3 = 1.65$) is mainly formed of plates, most being hexagonal in shape, but also consists of single crystals of which the shape is characteristic of $\text{Ca}_3[\text{Al}(\text{OH})_6]_2$,^{33,34} which was also identified in the XRD. As mentioned above, it is the intermediate for the LDH phase and was expected to be present in some degree. In either case, the formation of Ca–Al hydrates is important, as this ensures the desired homogeneous mixing of the Ca^{2+} and Al^{3+} ions in the support. For example, Li

et al.³⁵ showed that $\text{Ca}_3[\text{Al}(\text{OH})_6]_2$ (formed from $\text{Ca}(\text{OH})_2$ and $\text{Al}(\text{OH})_3$) can be used as a precursor for the synthesis of $\text{Ca}_{12}\text{Al}_{14}\text{O}_{33}$ at temperatures significantly lower than 1000 °C, probably because the Ca^{2+} and Al^{3+} ions are already well mixed at the molecular level.

3.2. Reduction–Oxidation Cycles in the TGA. The changes in mass of the sample and the measured temperature of the sample during the first two cycles of a typical experiment are presented in Figure 4. The sudden disturbance in mass at

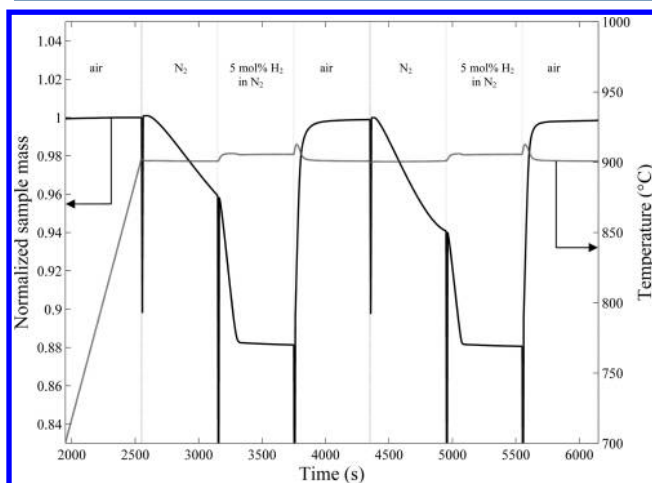


Figure 4. Typical weight change and temperature profiles obtained from the TGA, shown for the first two cycles (of 100) of batch 6 ($\text{CaO}/\text{Al}_2\text{O}_3 = 0.72$) at 900 °C. The sample was initially heated to 900 °C in air, prior to the first reduction at 2550 s.

the beginning of each reaction period is an artifact associated with the switching of gases. The duration of these disturbances was so short (typically less than 10 s) that they could be safely ignored.

The theoretical maximum oxygen capacity for the conversion of CuO to Cu , $R_{\text{OC,Cu,max}}$ for all eight oxygen carriers was 0.12 $\text{g}_{\text{O}_2}/\text{g}_{\text{OC}}$ (c.f. pure copper oxide that would be 0.20 $\text{g}_{\text{O}_2}/\text{g}_{\text{OC}}$) and was always achieved in each of the 100 redox cycles within the given reaction time. The theoretical oxygen capacity for CLOU, $R_{\text{OC,Cu}_2\text{O,max}}$ i.e., when only considering the oxygen release period in N_2 from CuO to Cu_2O , was 0.06 $\text{g}_{\text{O}_2}/\text{g}_{\text{OC}}$ assuming that the support remained totally inert and did not form any compounds with CuO , such as CuAl_2O_4 , as discussed above. For all OCs, the release of oxygen in the first cycle was always slower than in the subsequent cycles, e.g., the material in Figure 4 only reached 67% of the theoretical maximum oxygen capacity $R_{\text{OC,Cu}_2\text{O,max}}$ in the first cycle. After around three cycles, all the materials attained their full oxygen release capacity of $\sim 0.06 \text{ g}_{\text{O}_2}/\text{g}_{\text{OC}}$, viz. a normalized mass of 0.94 in Figure 4, within the reaction time allowed, and maintained this for all the subsequent cycles.

Unlike pure CuO , which is known to deactivate very quickly when exposed to alternating reducing and oxidizing conditions,³⁶ the OCs produced in this work showed little deterioration in their reactivity in the TGA during cycling. For example, the conversion profile during oxidation is shown in Figure 5 for batch 6 over 100 redox cycles. The rate of conversion, i.e., the gradient, was constant (except at very high conversions), and there was little change between cycles. For very active materials, rates of conversion in the TGA become

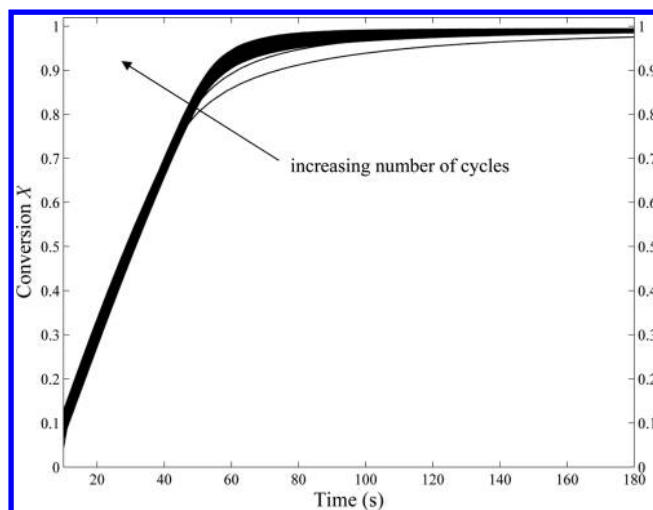


Figure 5. Conversion profiles as a function of time, obtained from measurements of the sample mass during the oxidation period (with air) in the TGA, using eq 1. In total, 100 cycles of reduction and oxidation were performed at 900 °C. Shown are the first 180 s of the oxidation reaction for batch 6 ($\text{CaO}/\text{Al}_2\text{O}_3 = 0.72$), after the disturbance caused by gas switching.

limited by the rate of diffusion of the reactant gas from the top of the crucible to the sample at its base. Thus, the TGA experiments are inconclusive and only provide a bound on the reactivity of the oxygen carrier. The maximum rate of reaction during oxidation at 900 °C can be calculated for nonequimolar diffusion in laminar flow in the crucible of the TGA. The crucibles had a diameter $d_c = 5 \text{ mm}$ (i.d.) and a depth $h = 4 \text{ mm}$.

$$N_{\text{O}_2} = C \cdot D_{\text{O}_2} \cdot \frac{\pi \cdot d_c^2}{4 \cdot h} \cdot \ln \frac{(1 - x_{\text{surface}})}{(1 - x_{\text{bulk}})} \quad (7)$$

In eq 7, N_{O_2} is the molar flow rate of O_2 (mol/s), C is the molar gas concentration (10.4 mol/m³), D_{O_2} is the molecular diffusivity of O_2 in N_2 ($2.2 \times 10^{-4} \text{ m}^2/\text{s}$), calculated from Chapman–Enskog theory for 900 °C,³⁷ $x_{\text{surface}} = 0.02$ and $x_{\text{bulk}} = 0.105$ (assuming 50% dilution of air with N_2 from the purge and protective gas). Multiplying N_{O_2} with M_{O_2} , the molecular weight of O_2 , yields the maximum rate of uptake of O_2 , 0.033 mg/s. The measured rate of reaction (from the slope of the oxidation curve shown in Figure 5) was $\sim 0.044 \text{ mg/s}$ and therefore governed by external mass transfer, within experimental error.

Similarly, the maximum rate of reaction during reduction can be calculated for equimolar counter diffusion.

$$N_{\text{H}_2} = C \cdot D_{\text{H}_2} \cdot \frac{\pi \cdot d_c^2}{4 \cdot h} \cdot x_{\text{H}_2} \quad (8)$$

where N_{H_2} is the molar flow rate of H_2 (mol/s) and D_{H_2} is the molecular diffusivity of H_2 in N_2 ($7.3 \times 10^{-4} \text{ m}^2/\text{s}$ at 900 °C). Assuming again 50% dilution of the reactive gas with the inert purge and protective gases, x_{H_2} , the mole fraction of H_2 , is 0.025. Multiplying N_{H_2} with M_{O_2} and taking into account the stoichiometry of the reduction reaction of the CuO with H_2 , yields the maximum rate of loss of O_2 , $r_{\text{max,O}_2,\text{reduction}}$ ($\text{g}_{\text{O}_2}/\text{s}$), when oxidizing the H_2 under diffusion control.

$$r_{\max, \text{O}_2, \text{reduction}} = 0.5 \cdot C \cdot D_{\text{H}_2} \cdot \frac{\pi \cdot d_c^2}{4 \cdot h} \cdot x_{\text{H}_2} \cdot M_{\text{O}_2} \quad (9)$$

Hence, $r_{\max, \text{O}_2, \text{reduction}}$ is 0.015 mg/s. This compares to ~ 0.011 mg/s for the measured rate of reaction, so that during both oxidation and reduction, the rates of conversion were very close to those expected.

This implies that both oxidation and reduction reactions in these experiments were fast, and that all that can be concluded is that the materials studied did not deactivate sufficiently for the experiments to be limited by anything other than mass transfer. The only exception to this behavior was in the first few cycles and at high conversions, where the rate of oxidation appeared to increase with cycling (to the mass transfer limit).

3.3. Fluidized Bed Cycling Experiments. In the fluidized bed, particles are subjected to mechanical stresses. Batch 1, with the lowest content of calcium in the support, was found to have poor mechanical stability and gave a high rate of attrition, so it was excluded from this investigation. The other seven materials were found to be suitable for the fluidized bed reactor. In total, more than 90 cycling experiments were carried out, corresponding to almost 600 h of fluidization.

The measurements of the bed temperature and the off-gas concentrations from a typical experiment at 900 °C are shown in Figure 6 for batch 5. Again, for clarity, only the first two cycles are plotted.

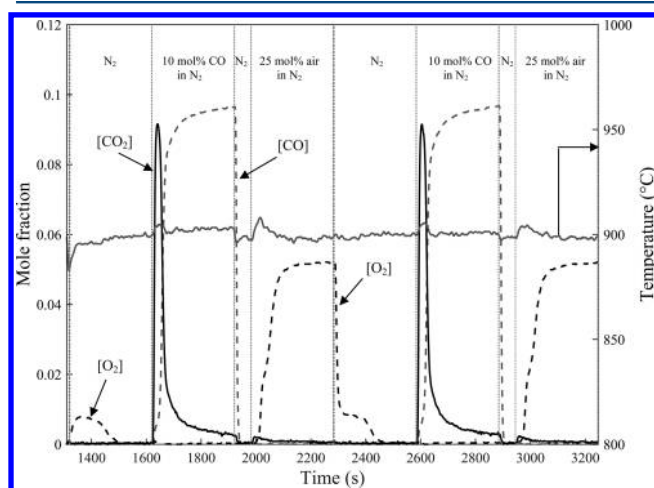


Figure 6. Typical concentration profiles of CO_2 , CO and O_2 for the first two (of 25) cycles when OC batch 5 ($\text{CaO}/\text{Al}_2\text{O}_3 = 0.55$) was cycled at ~ 900 °C in the fluidized bed.

As can be seen from the measured off-gas concentration of oxygen, the release of oxygen during the inert period was fast, and complete conversion $X_{\text{red}, \text{CuO}-\text{Cu}_2\text{O}} \sim 0.5$ was achieved. During the reduction using 10 mol % CO, the OC was completely reduced to Cu, and the reaction was sufficiently fast initially to consume most of the CO entering the reactor. It should be noted that at the end of the reduction phase in Figure 6, the CO_2 concentration did not return to zero owing to unwanted side reactions of the inlet gases with the reactor materials. These reactions were accounted for by subtracting the off-gas concentrations obtained from blank runs with a bed of pure silica sand, such that the conversions could be calculated accurately. The oxidation of the OC was also fast and initially limited by the availability of oxygen entering the reactor. Thus, the fluidized bed did not operate as a differential

reactor and the rates of OC conversion, and the shapes of the curves of conversion vs time (which determines the final capacity after a given time) reflect a combination of factors, including sampling system, mass transfer, reactant supply and intrinsic kinetics, where only the latter changes when a material “deactivates”. In fact, as noted below, in many cases the state of the OC material had little effect on the observed rate, so that changes in the profile of conversion vs time only became apparent once the material had deactivated sufficiently. Thus, all things being equal, and provided the kinetics are slow enough to have some impact on the rate of conversion, the changes in the shape of the curve or the time to reach a given conversion, can be used to compare the different batches.

Effect of Temperature on the Cyclic Performance. Figure 7 shows the conversion profile for batch 3 as a function of time

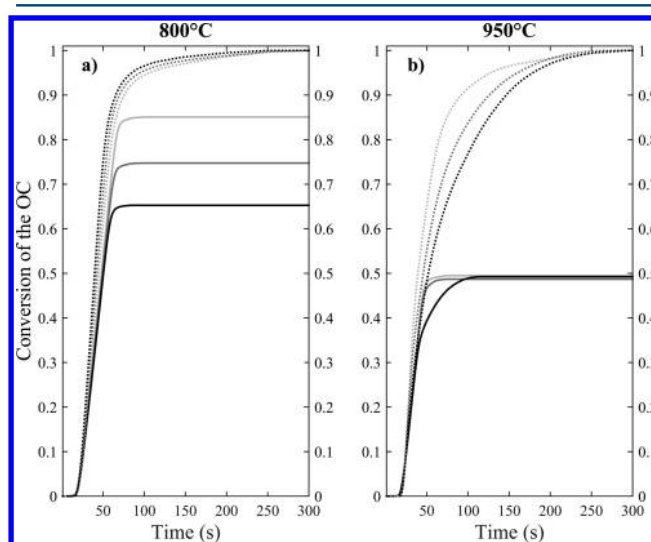


Figure 7. Conversion profiles obtained from measurements of the off-gas concentration from the FBR during a cycling experiment with batch 3 ($\text{CaO}/\text{Al}_2\text{O}_3 = 0.28$): (a) at 800 °C and (b) at 950 °C. Solid lines represent the conversion during the reduction reaction with 10 mol % CO in N_2 , dashed lines represent the normalized conversion during the oxidation reaction with 25 mol % air in N_2 (800 °C) and 50 mol % air in N_2 (950 °C). The colors correspond to the number of the reaction cycle: cycle 5 (light gray), cycle 15 (gray) and cycle 25 (black).

for the reduction using 10 mol % CO (solid lines), $X_{\text{red}, \text{CuO}-\text{Cu}}$ and the oxidation (dashed lines), X_{ox} at 800 and 950 °C.

At 800 °C, the oxygen release, which preceded the reduction, was slow, and the OC was not fully reduced to Cu_2O in the period allowed. Therefore, the ultimate conversion during reduction, $X_{\text{red}, \text{CuO}-\text{Cu}}$ exceeded 0.5 and also decreased with an increase in cycle number. The rate of reduction with 10 mol % CO was significantly faster than the rate of decomposition during the CLOU period, and resulted in complete reduction of the mixture of CuO and Cu_2O . In fact, the rate of reduction was so fast that it was limited by the availability of CO entering the reactor. This, in conjunction with the slow response of the gas analyzer and sampling system, dominated the shape of the conversion–time profile. The amount of oxygen released during the CLOU stage in the finite time allowed increased somewhat with cycling and stabilized after ~ 2 –3 cycles at an ultimate conversion $X_{\text{red}, \text{CuO}-\text{Cu}_2\text{O}} \sim 0.12$. The measured off-gas mole fraction of O_2 after 3 cycles was relatively constant (~ 0.001), indicating that the rate of conversion was limited by

the equilibrium (the theoretical mole fraction of O_2 for the transition of CuO to Cu_2O at $800\text{ }^\circ\text{C}$ is ~ 0.0013). The initial increase in apparent rate of oxygen release was also seen in the TGA. Ideally, the sum of the final values of $X_{red,CuO-Cu_2O}$ and $X_{red,CuO-Cu}$ should be unity, i.e., full conversion of CuO to Cu . The sum of both values of conversion after 5 cycles was ~ 0.97 , after 15 cycles ~ 0.87 and after 25 cycles ~ 0.77 . The profiles of conversion during oxidation gave ultimate conversions in line with $X_{red,CuO-Cu_2O} + X_{red,CuO-Cu}$ but have been normalized in Figure 7 to show that while the ultimate conversions have fallen, the shape of the curve remained similar, indicating that at this temperature the deactivation in the performance in batch 3 was largely owing to loss of material from the reactor. The mechanical stability of batch 3 was rather poor and after ~ 7 h of fluidization, almost 25 wt % of the OC was elutriated.

At $950\text{ }^\circ\text{C}$, the conversion of CuO to Cu_2O was complete in every cycle. Therefore, the maximum value of $X_{red,CuO-Cu}$ possible was 0.5. The oxidation was initially faster than the reduction, but both showed decreasing rates of conversion with cycling, as opposed to those obtained at $800\text{ }^\circ\text{C}$. The loss of material at $950\text{ }^\circ\text{C}$ was significantly lower than at $800\text{ }^\circ\text{C}$, ~ 2 wt %, assuming the loss in capacity can be entirely attributed to attrition.

The other materials also followed, qualitatively, the trends shown in Figure 7, with the main difference being that at $800\text{ }^\circ\text{C}$ those batches prepared with higher mass ratios of CaO to Al_2O_3 in the support showed less attrition. The reduction in 10 mol % CO always went to completion within the given reaction time and the experiments at $800\text{ }^\circ\text{C}$ therefore provided a good method of evaluating the resistance toward attrition. In this case the apparent loss of oxygen capacity, i.e., $(1 - X_{red,CuO-Cu} - X_{red,CuO-Cu_2O})$, can be attributed to material loss. $X_{red,CuO-Cu_2O}$ was always ~ 0.12 after 300 s in N_2 and should not have been affected by any loss of material, as the oxygen release reaction was still limited by the equilibrium and $X_{red,CuO-Cu_2O}$ was much smaller than 0.5. After 25 cycles at $800\text{ }^\circ\text{C}$, $X_{red,CuO-Cu}$ varied from ~ 0.65 for batch 2 and batch 3 to ~ 0.87 for batch 8, which translates into losses of material of ~ 23 and ~ 1 wt %, respectively. At $950\text{ }^\circ\text{C}$, the decreasing rates of conversion for both the reduction and oxidation reactions were consistent for all OCs investigated, but to a lesser extent for those materials prepared with lower CaO/Al_2O_3 .

Cyclic Performance of the Different Oxygen Carriers. Figure 8 shows how the $X_{red,CuO-Cu}$ vs time varied with cycle for batches 2, 5, 6 and 8 at $900\text{ }^\circ\text{C}$. The shape of the curves for batch 2 are similar to those shown in Figure 7 at $800\text{ }^\circ\text{C}$ for batch 3, and the drop in the final value of $X_{red,CuO-Cu}$ with cycle number can again be explained by loss of material due to attrition and subsequent elutriation of the fines. The slope of the curve for $X_{red,CuO-Cu} < \sim 0.3$ did not change significantly with the number of cycles, indicating that the initial rate of conversion was fast and most likely affected by the slow response of the sampling system. For batch 5, the shape of the conversion vs time curves remained almost unchanged for 25 cycles. The rate of conversion in cycle 1 for batch 6 was slightly slower than that of batches 2 and 5, but drastically decreased after only one cycle and remained relatively constant from around cycle 5. Batch 8, with an even higher mass ratio of CaO to Al_2O_3 in the support, showed a similar behavior as batch 6; however, the drop of the rate of conversion was not as significant. Interestingly, the rate of oxygen release for batch 8 was slower than that for batch 6 in the first cycle and

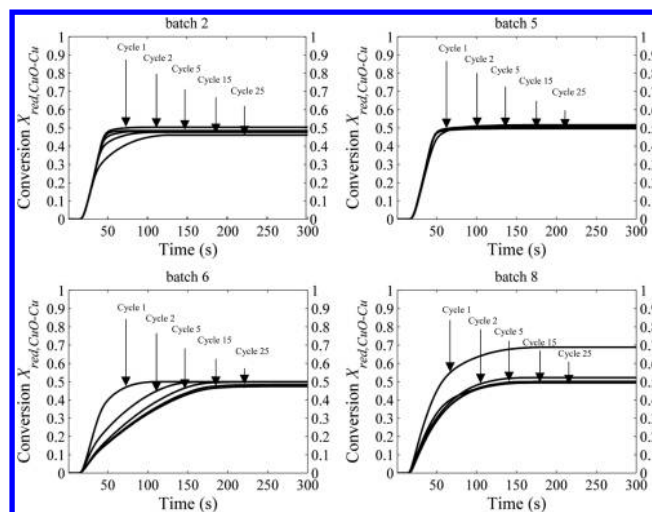


Figure 8. Conversion profiles for $X_{red,CuO-Cu}$ obtained from measurements of the off-gas concentration from the FBR during cycling experiments with batch 2 ($CaO/Al_2O_3 = 0.22$), batch 5 ($CaO/Al_2O_3 = 0.55$), batch 6 ($CaO/Al_2O_3 = 0.72$) and batch 8 ($CaO/Al_2O_3 = 1.65$) during the reduction period with 10 mol % CO in N_2 at $900\text{ }^\circ\text{C}$.

incomplete, as seen from $X_{red,CuO-Cu}$ that exceeded 0.5 in cycle 1.

From the plots of conversion vs time, the cyclic behavior of the OCs investigated fell into two broad categories, discussed in section 4; one characterized by a sudden initial drop in reactivity (batches 6–8), corresponding to an increase in time to reach full conversion, the other one by a relatively stable cyclic performance (batches 2–5).

Images of the particles recovered after 25 cycles are shown in Figure 9. As with the cyclic performance, the particles tended to fall into one of two groups; either they appeared almost unchanged in size and shape from the fresh particles, e.g., batches 2 and 5 in Figure 9a,b, or they formed agglomerates (batches 6 and 8 in Figure 9c,d). Thus, the changes in reactivity seen in Figure 8 correlated with whether or not the particles agglomerated. The extent of the formation of agglomerates for batches 6 to 8 was solely dependent on the composition of the OC, not the temperature, over the range 800 to $950\text{ }^\circ\text{C}$. In Figure 9 a, small fragments could be identified, in agreement with the high rates of mass loss observed for materials with a low CaO/Al_2O_3 .

3.4. Characterization of the Oxygen Carriers as Prepared. The effect of the calcium content in the support was studied in more detail by XRD, after the oxygen carriers had been calcined at $1000\text{ }^\circ\text{C}$ for 6 h (Figure 10). It was also confirmed by XRD, not shown here, that the duration of the calcination (6, 12 or 24 h) did not make any difference with respect to which phases were formed and to what extent.

In theory, upon calcination different phases of calcium aluminates should have formed, depending on the amounts of CaO and Al_2O_3 present in the support.³⁸ The software package NPL mtdata³⁹ was used for thermodynamic calculations to predict the formation of the different phases for the system $CuO-CaO-Al_2O_3$ at $1000\text{ }^\circ\text{C}$. From the calculations, the formation of $CuAl_2O_4$ is thermodynamically feasible when the mass ratio of CaO to Al_2O_3 is < 0.28 , i.e., for batches 1 and 2. The calcium aluminate phase that would have been expected to form for such low mass ratios of CaO to Al_2O_3 , $CaAl_{12}O_{19}$, is thermodynamically unstable at $1000\text{ }^\circ\text{C}$; instead $CaAl_4O_7$ is

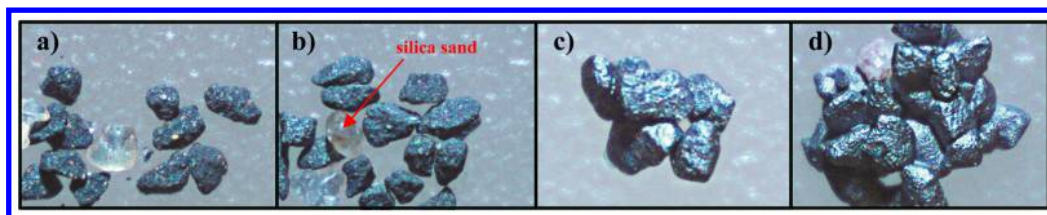


Figure 9. Microscope images of collected oxygen carrier particles from the FBR after 25 redox cycles at 900 °C, at a magnification of 60×: (a) batch 2 ($\text{CaO}/\text{Al}_2\text{O}_3 = 0.22$), (b) batch 5 ($\text{CaO}/\text{Al}_2\text{O}_3 = 0.55$), (c) batch 6 ($\text{CaO}/\text{Al}_2\text{O}_3 = 0.72$) and (d) batch 8 ($\text{CaO}/\text{Al}_2\text{O}_3 = 1.65$).

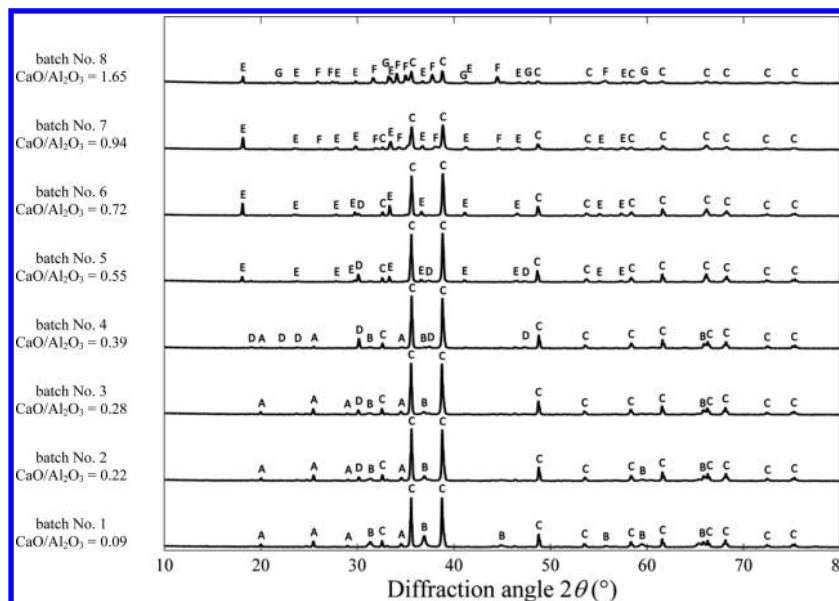


Figure 10. X-ray diffraction patterns of the eight oxygen carriers investigated, after calcination at 1000 °C for 6 h. The peaks corresponding to crystalline phases were labeled as (A) CaAl_4O_7 , (B) CuAl_2O_4 , (C) CuO , (D) CaAl_2O_4 , (E) $\text{Ca}_{12}\text{Al}_{14}\text{O}_{33}$, (F) $\text{Ca}_3\text{Cu}_7\text{O}_{10}$ and (G) $\text{Ca}_3\text{Al}_2\text{O}_6$.

predicted to form. For batches 3 to 8, CuO is the only Cu phase existing in equilibrium with the calcium aluminate phases.

The TGA results suggest that there was no detectable interaction of the CuO with the support. However, in batches 1 to 4, CuAl_2O_4 was detected by XRD, and is known to diminish the effective oxygen release capacity $R_{\text{OC,Cu}_2\text{O}}$.^{11,12} CuAl_2O_4 is fully reducible by CO , and although it is the stable phase when CuO and Al_2O_3 coexist, its rate of formation is rather slow.⁴⁰ The XRD pattern of batch 2 that had been fully reduced and reoxidized once at 900 °C (not shown here) did not contain any significant peaks corresponding to the CuAl_2O_4 phase, as opposed to the fresh batch 2 (labeled as B in Figure 10). This indicates that, upon cycling, the quantity of CuAl_2O_4 formed during the oxidation reaction was negligible in comparison with the amount of CuO present, resulting in values of $R_{\text{OC,Cu}_2\text{O}}$ being close to $R_{\text{OC,Cu}_2\text{O,max}}$.

The calcium aluminate phases formed are summarized in Table 1 and corresponded to the phases expected from the phase diagram for the $\text{Ca}-\text{Al}-\text{O}$ system.^{26,38} The intensities of the CuO peaks (C) in Figure 10 are relatively constant, but decrease from batch 6 to batch 8, i.e., on increasing the calcium content. In these patterns, a new phase could be identified, $\text{Ca}_3\text{Cu}_7\text{O}_{10}$.⁴¹ For comparison, a sample of CuO (60 wt %) and CaO (40 wt %) was synthesized using the method described previously, i.e., excluding the $\text{Al}(\text{OH})_3$. The phases identified for this sample, which was heavily sintered and appeared to have gone through a molten phase, were $\text{Ca}_3\text{Cu}_7\text{O}_{10}$, Ca_2CuO_3 and CuO . In Figure 10, the phase corresponding to Ca_2CuO_3

was absent, probably owing to the high ratio of CuO/CaO , and only $\text{Ca}_3\text{Cu}_7\text{O}_{10}$ was seen.

Tsang et al.⁴¹ investigated the $\text{CaO}-\text{CuO}$ system and found that the stable phases above 980 °C, close to the calcination temperature of the OCs in the present work, were Ca_2CuO_3 and $\text{Ca}_3\text{Cu}_7\text{O}_{10}$. They further noted that the phase CaCu_2O_3 reported by others,⁴² was likely to be erroneously identified as such, and was in fact the phase $\text{Ca}_3\text{Cu}_7\text{O}_{10}$.

In Figure 11, SEM images are shown for samples that were prepared without the CuO and calcined for 6 h at 800 °C (a–c) and 1000 °C (d–f), respectively.

At 800 °C, the morphologies of batches 2, 5 and 8 look remarkably similar to that shown in Figure 3, i.e., before calcination. Both the interlocking crystals in batch 5 and the plates corresponding to the LDH phase in batch 8 are maintained. In batch 8, the single crystals arising from the $\text{Ca}_3[\text{Al}(\text{OH})_6]_2$ are predominant, whereas the hexagonal plates appeared to have partly disintegrated. At 1000 °C, the morphology of the three batches is of no particular order and the structure initially present has been completely destroyed.

4. DISCUSSION

In the TGA, all the OCs maintained or even improved their cyclic performance. However, if the reaction is very fast, the inherent mass transfer limitations in the TGA mean that changes in reaction rate are not seen. The cycle time used in the TGA was always sufficient to obtain complete reduction and oxidation of the materials investigated. Furthermore, the

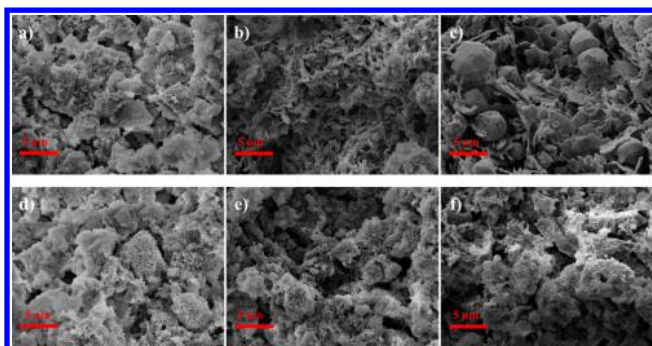


Figure 11. Scanning electron microscope images at a magnification of 10000 \times , after calcination at 800 $^{\circ}\text{C}$ (a–c) and 1000 $^{\circ}\text{C}$ (d–f), respectively. (a, d) batch 2 ($\text{CaO}/\text{Al}_2\text{O}_3 = 0.22$), (b, e) batch 5 ($\text{CaO}/\text{Al}_2\text{O}_3 = 0.55$) and (c, f) batch 8 ($\text{CaO}/\text{Al}_2\text{O}_3 = 1.65$). The materials were prepared without CuO.

particles in the TGA are not subjected to the same mechanical stresses seen in a fluidized bed, and the effects of agglomeration may not be seen in a TGA if only a small number of particles are used.

In the fluidized bed, some changes in performance of the OCs were seen with cycling. At the highest temperatures studied, batch 3 ($\text{CaO}/\text{Al}_2\text{O}_3 = 0.28$) did not agglomerate or attrit significantly, but the observed rate of conversion decreased relative to that seen at 800 $^{\circ}\text{C}$. The fact that both an increase in mechanical stability, i.e., a resistance to attrition, and a decrease in reactivity was observed at higher reaction temperatures (950 $^{\circ}\text{C}$) for all materials may not be a coincidence. Thus, the apparent decrease in OC reactivity was probably owing to sintering processes during the reduction stage, when the OC was reduced to Cu. Sintering is likely to be accompanied by local surface melting of the grains and a densification of the material, which results in an increase in mechanical stability.

The slow response of the gas sampling system and mass transfer limitations made it difficult to assess the detailed kinetics of the materials. In a separate experiment, not presented in this work but similar to that described by Chuang et al.⁴³ under conditions that were less limited by external mass transfer, reactant supply or analyzer response, the rates of the reduction reaction for materials equivalent in composition to batches 4 and 7 were measured.⁴⁴ The material used had been cycled 25 times at 900 $^{\circ}\text{C}$ under the conditions described in Section 2.2 and was compared to fresh OC. The observed rates of reaction for both batches 4 and 7 were higher after the 25 cycles of reduction and oxidation in a fluidized bed. Thus, at a particle scale, the reactivity of the material did not deteriorate over the 25 cycles, but had become more limited by diffusion through and to the large agglomerates that formed, as shown in Figure 9.

XRD measurements of the calcined particles before reaction showed that the calcium aluminate phases formed were largely those expected from the Ca–Al–O phase diagram and the thermodynamic calculations. This suggests that the composition of the support was relatively homogeneous, which would not be expected if it were prepared by mixing powders at this low temperature.⁴⁵ The good interaction between the Ca- and Al-species arose from the hydration reaction of the $\text{Ca}(\text{OH})_2$ and $\text{Al}(\text{OH})_3$ that subsequently, with the CO_2 from the atmosphere, formed Ca–Al hydrates and an LDH phase identified as calcium monocarboaluminate hydrate. The extent

of the formation of the Ca–Al LDH was dependent on the ratio of $\text{Ca}(\text{OH})_2$ to $\text{Al}(\text{OH})_3$, as detected in the XRD. The SEM images suggest that the plate-like structure was not maintained after the calcination and did therefore not contribute to the higher mechanical stability compared to those batches with initially less LDH present.

At mass ratios of CaO to $\text{Al}_2\text{O}_3 > 0.94$, the XRD patterns of the materials clearly show the formation of a new phase, and the loss of some CuO to what appears to be a mixed calcium–copper oxide, identified as $\text{Ca}_3\text{Cu}_7\text{O}_{10}$. Thus, for batch 8, instead of pure $\text{Ca}_3\text{Al}_2\text{O}_6$ a mixture of $\text{Ca}_3\text{Al}_2\text{O}_6$ and $\text{Ca}_{12}\text{Al}_{14}\text{O}_{33}$ formed. Investigations of the kinetics of formation of calcium aluminates by Singh et al.⁴⁶ and Mohamed and Sharp⁴⁷ concluded that $\text{Ca}_3\text{Al}_2\text{O}_6$ was formed by the reaction between CaO and the reaction intermediates, primarily $\text{Ca}_{12}\text{Al}_{14}\text{O}_{33}$. This was clearly seen in the XRD (not shown here) when the support of batch 8, i.e., without the CuO, had been calcined for both 6 and 24 h at 1000 $^{\circ}\text{C}$, resulting primarily in the formation of $\text{Ca}_{12}\text{Al}_{14}\text{O}_{33}$ and CaO in either case, with only a little $\text{Ca}_3\text{Al}_2\text{O}_6$ being formed. The mixed calcium–copper oxides have previously been shown to be readily formed by solid-state sintering of CuO and CaO at temperatures as low as 970 $^{\circ}\text{C}$ (in air) within 4 h.¹⁵ This indicates that at ~ 1000 $^{\circ}\text{C}$, the kinetics of the formation of the $\text{Ca}_3\text{Cu}_7\text{O}_{10}$ phase are faster than those of the formation of $\text{Ca}_3\text{Al}_2\text{O}_6$, and that some of the CuO reacted with CaO that existed alongside the reaction intermediates. The phase diagram for the Ca–Cu–O system indicates that not only can mixed oxides form⁴¹ but also that these can melt at lower temperatures than CuO, Cu_2O or Cu alone. These phases with relatively low melting temperatures also caused the densification of the material, resulting in an increase in the measured bulk density (as seen in Table 1). Also, batches 6 and 7 had much higher densities than batches 1 to 5. In batches 6 and 7, the LDH phase ($\text{Ca}_4\text{Al}_2\text{O}_6(\text{CO}_3)11\text{H}_2\text{O}$) was still significant before calcination. When the LDH phase thermally decomposes, there probably exists locally excess of calcium ions relative to the molar ratio $\text{Ca}^{2+}/\text{Al}^{3+}$ required to form the desired calcium aluminate phases; hence, the mechanism of the formation of the calcium–copper oxides in batches 6 and 7 might be similar to that proposed for batch 8. According to the literature, the $\text{Ca}_3\text{Al}_2\text{O}_6$ and $\text{Ca}_{12}\text{Al}_{14}\text{O}_{33}$ phases may thus also be transition phases for the lower calcium aluminate phases, so that free CaO can react with the CuO.^{16,35,48}

Therefore, it seems likely that in the materials with a mass ratio of CaO to $\text{Al}_2\text{O}_3 \geq 0.72$ in the support, i.e., from batch 6, interaction of the CuO with CaO from the support resulted in the formation of binary oxides of low melting point, leading to sintering during the initial calcination (giving a lower initial reactivity but strong particles), and agglomeration during cycling. To avoid the interaction of the CuO with the CaO during calcination, the amount of CaO in the support must therefore be limited such that the mass ratio of CaO to $\text{Al}_2\text{O}_3 < 0.72$, i.e., when the formation of the LDH phase (and therefore the formation of calcium aluminate hydrate phases) becomes less significant. On the other hand, the presence of these hydrates is also desired, as they guarantee homogeneous mixing of the Ca^{2+} and Al^{3+} ions in the starting materials, $\text{Ca}(\text{OH})_2$ and $\text{Al}(\text{OH})_3$, at the molecular level.

In this work, batches 4 and 5 performed best, corresponding to mass ratios of CaO to Al_2O_3 in the support of 0.39 and 0.55, respectively. In both materials, the Ca–Al LDH phase was present that resulted in a morphology of interlocking crystals

that appeared to have stabilized the OC mechanically after drying. After the calcination at 1000 °C, the beneficial structure disintegrated, but may still have been more stable than that of the batches prepared with lower mass ratios of CaO to Al₂O₃. Those batches were found to be too fragile for long-term usage in fluidized beds.

5. CONCLUSIONS

Eight different CuO-based oxygen carriers supported on calcium aluminates were synthesized by a wet-mixing method and their cyclic performance was evaluated over 100 cycles of reduction and oxidation for a temperature range of 800 to 950 °C. The method of preparation involved the formation of calcium aluminum hydrate phases, which transformed into Ca–Al LDH and ensured homogeneous mixing of the Ca²⁺ and Al³⁺ ions at the molecular level.

In the TGA, all OCs maintained their chemical reactivity over the 100 redox cycles. Within the limitations of the TGA setup, no significant interactions of the CuO with the cementitious support could be identified, or at the very least no interaction that reduced the amount of oxygen available. In the FBR, the OCs were exposed to harsher reaction conditions that, in some cases, resulted in significant differences in the cyclic performance compared with the TGA. OCs prepared with a mass ratio of CaO to Al₂O₃ > 0.55 in the support sintered upon calcination and agglomerated in the fluidized bed, resulting in a decrease in cyclic performance. Despite agglomeration, which happened in the early stages of an experiment, the apparent reactivity of the OCs was still high and full conversion (from CuO to Cu and *vice versa*) was achieved. Separate experiments in a fluidized bed, in which the rates were partly controlled by chemical kinetics, showed that rather than deactivating, the rates of reduction of two of the materials improved after 25 cycles at 900 °C. Therefore, the deactivation seen in the cycling experiments can be mainly attributed to agglomeration of the particles, increasing internal and exterior resistance to mass transfer. There is evidence that the origin of the sintering is the interaction of CuO with CaO forming calcium–copper oxide phases with relatively low melting points. This did not appear to occur when the mass ratio of CaO to Al₂O₃ in the support was ≤0.55.

AUTHOR INFORMATION

Corresponding Author

*F. Donat. E-mail: fd299@cam.ac.uk.

Notes

The authors declare no competing financial interest.

ACKNOWLEDGMENTS

The authors thank Mohammad Ismail and Matthew Dunstan for helping with the XRD analysis and Alex Casabuena-Rodriguez and for helping with the SEM. This work was supported by the Engineering and Physical Sciences Research Council (EPSRC grant EP/I010912/1).

REFERENCES

- (1) Mattisson, T.; Lyngfelt, A.; Leion, H. Chemical-looping with oxygen uncoupling for combustion of solid fuels. *Int. J. Greenhouse Gas Control* **2009**, *3*, 11–19.
- (2) Leion, H.; Mattisson, T.; Lyngfelt, A. Using chemical-looping with oxygen uncoupling (CLOU) for combustion of six different solid fuels. *Energy Procedia* **2009**, *1*, 447–453.

- (3) Eyring, E. M.; Konya, G.; Lighty, J. S.; Sahir, A. H.; Sarofim, A. F.; Whitty, K. J. Chemical looping with copper oxide as carrier and coal as fuel. *Oil Gas Sci. Technol.* **2011**, *66*, 209–221.

- (4) Ströhle, J.; Orth, M.; Epple, B. Design and operation of a 1 MW_{th} chemical looping plant. *Appl. Energy* **2014**, *113*, 1490–1495.

- (5) Thon, A.; Kramp, M.; Hartge, E. U.; Heinrich, S.; Werther, J. Operational experience with a system of coupled fluidized beds for chemical looping combustion of solid fuels using ilmenite as oxygen carrier. *Appl. Energy* **2014**, *118*, 309–317.

- (6) Peterson, S. B.; Konya, G.; Clayton, C. K.; Lewis, R. J.; Wilde, B. R.; Eyring, E. M.; Whitty, K. J. Characteristics and CLOU performance of a novel SiO₂-supported oxygen carrier prepared from CuO and β-SiC. *Energy Fuels* **2013**, *27*, 6040–6047.

- (7) Adanez, J.; Abad, A.; Gracia-Labiano, F. Progress in chemical-looping combustion and reforming technologies. *Prog. Energy Combust. Sci.* **2012**, *38*, 215–282.

- (8) Xu, L.; Wang, J.; Li, Z.; Cai, N. Experimental study of cement-supported CuO oxygen carriers in chemical looping with oxygen uncoupling (CLOU). *Energy Fuels* **2013**, *27*, 1522–1530.

- (9) Manovic, V.; Anthony, E. J. Integration of calcium and chemical looping combustion using composite CaO/CuO-based materials. *Environ. Sci. Technol.* **2011**, *45*, 10750–10756.

- (10) Dennis, J. S.; Pacciani, R. The rate and extent of uptake of CO₂ by a synthetic, CaO-containing sorbent. *Chem. Eng. Sci.* **2009**, *64*, 2147–2157.

- (11) Arjmand, M.; Azad, A.; Leion, H.; Mattisson, T.; Lyngfelt, A. Evaluation of CuAl₂O₄ as an oxygen carrier in chemical-looping combustion. *Ind. Eng. Chem. Res.* **2012**, *51*, 13924–13934.

- (12) Imtiaz, Q.; Broda, M.; Müller, C. R. Structure-property relationship of co-precipitated Cu-rich, Al₂O₃- or MgAl₂O₄-stabilized oxygen carriers for chemical looping with oxygen uncoupling (CLOU). *Appl. Energy* **2014**, *119*, 557–565.

- (13) Song, Q.; Liu, W.; Bohn, C. D.; Harper, R. N.; Sivaniah, E.; Scott, S. A.; Dennis, J. S. A high performance oxygen storage material for chemical looping processes with CO₂ capture. *Energy Environ. Sci.* **2013**, *6*, 288–298.

- (14) Imtiaz, Q.; Kierzkowska, A. M.; Müller, C. R. Coprecipitated, copper-based, alumina-stabilized materials for carbon dioxide capture by chemical looping combustion. *ChemSusChem* **2012**, *5*, 1610–1618.

- (15) Li, Q. S.; Zhang, Y. Q.; Li, L. B.; Zang, G. Z. Dielectric properties of Ca₂CuO₃–CaCu₂O₃–CuO composite ceramics. *Mod. Phys. Lett. B* **2013**, *27*, 1350042.

- (16) Taylor, H. F. W. *Cement Chemistry*; Thomas Telford: London, 1997.

- (17) Francois, M.; Renaudin, G.; Evrard, O. A cementitious compound with composition 3CaO·Al₂O₃·CaCO₃·11H₂O. *Acta Crystallogr., Sect. C: Cryst. Struct. Commun.* **1998**, *54*, 1214–1217.

- (18) Chang, P. H.; Chang, Y. P.; Chen, S. Y.; Yu, C. T.; Chyou, Y. P. Ca-Rich Ca–Al-oxide, high-temperature-stable sorbents prepared from hydrotalcite precursors: Synthesis, characterization, and CO₂ capture capacity. *ChemSusChem* **2011**, *4*, 1844–1851.

- (19) Sauman, Z.; Lach, V. Long-term carbonization of the phases 3CaO·Al₂O₃·6H₂O and 3CaO·Al₂O₃·SiO₂·4H₂O. *Cem. Concr. Res.* **1972**, *2*, 435–446.

- (20) Scrivener, K. L.; Cabiron, J. L.; Letourneux, R. High-performance concretes from calcium aluminate cements. *Cem. Concr. Res.* **1999**, *29*, 1215–1223.

- (21) Black, L.; Breen, C.; Yarwood, J.; Deng, C. S.; Phipps, J.; Maitland, G. Hydration of tricalcium aluminate (C3A) in the presence and absence of gypsum-studied by Raman spectroscopy and X-ray diffraction. *J. Mater. Chem.* **2006**, *16*, 1263–1272.

- (22) Lothenbach, B.; Pelletier-Chaignat, L.; Winnefeld, F. Stability in the system CaO–Al₂O₃–H₂O. *Cem. Concr. Res.* **2012**, *42*, 1621–1634.

- (23) Pfeiffer, H.; Avalos-Rendon, T.; Lima, E.; Valente, J. Thermochemical and cyclability analyses of the CO₂ absorption process on a Ca/Al layered double hydroxide. *J. Environ. Eng.* **2011**, *137*, 1058–1065.

- (24) Xu, S.; Zhang, B.; Chen, Z.; Yu, J.; Evans, D. G.; Zhang, F. A general and scalable formulation of pure CaAl-layered double

hydroxide via an organic/water solution route. *Ind. Eng. Chem. Res.* **2011**, *50*, 6567–6572.

(25) Duan, X.; Evans, D. G. *Layered Double Hydroxides*; Springer: New York, 2006.

(26) Hallstedl, B. Assessment of the CaO-Al₂O₃ System. *J. Am. Ceram. Soc.* **1990**, *73*, 15–23.

(27) Barret, P.; Bertrandie, D.; Beau, D. Calcium hydrocarboaluminate, carbonate, alumina gel and hydrated aluminates solubility diagram calculated in equilibrium with CO_{2g} and with Na_{aq}⁺ ions. *Cem. Concr. Res.* **1983**, *13*, 789–800.

(28) Grandet, J.; Ollivier, J. P. Etude de la formation du monocarboaluminate de calcium hydrate au contact d'un granulats calcaire dans une pate de ciment portland. *Cem. Concr. Res.* **1980**, *10*, 759–770.

(29) McCarter, W. J. Gel formation during early hydration. *Cem. Concr. Res.* **1987**, *17*, 55–64.

(30) Sathiyamoorthy, D.; Sridhar Rao, C. The choice of distributor to bed pressure drop ratio in gas fluidised beds. *Powder Technol.* **1981**, *30*, 139–143.

(31) Kunii, D.; Levenspiel, O. *Fluidization Engineering*; Wiley: New York, 1991.

(32) Renaudin, G.; Francois, M.; Evrard, O. Order and disorder in the lamellar hydrated tetracalcium monocarboaluminate compound. *Cem. Concr. Res.* **1999**, *29*, 63–69.

(33) Breval, E. C3A hydration. *Cem. Concr. Res.* **1976**, *6*, 129–137.

(34) Sánchez-Herrero, M. J.; Fernández-Jiménez, A.; Palomo, A. Alkaline hydration of tricalcium aluminate. *J. Am. Ceram. Soc.* **2012**, *95*, 3317–3324.

(35) Li, C.; Hirabayashi, D.; Suzuki, K. Synthesis of higher surface area mayenite by hydrothermal method. *Mater. Res. Bull.* **2011**, *46*, 1307–1310.

(36) Diego, L. F.; Garcia-Labiano, F.; Adánez, J.; Gayán, P.; Abad, A.; Corbella, B. M.; Palacios, J. M. Development of Cu-based oxygen carriers for chemical-looping combustion. *Fuel* **2004**, *83*, 1749–1757.

(37) Cussler, E. L. *Diffusion: Mass Transfer in Fluid Systems*; Cambridge University Press: Cambridge, U. K., 2009.

(38) Waring, J. L.; Roth, R. S.; Brower, W. S.; Harding, C. A. Investigation of calcium aluminate cement phases under high gaseous pressure. *J. Res. Natl. Bur. Stand. (U. S.)* **1977**, *82*, 167–172.

(39) Davies, R.; Dinsdale, A.; Chart, T. Application of MTDATA to the modeling of multicomponent equilibria; *Materials Chemistry at High Temperatures*, Vol. 1; Humana Press: New York, 1990.

(40) Paulsson, H.; Rosén, E. A study of the formation of CuAl₂O₄ from CuO and Al₂O₃ by solid state reaction at 1000 °C and 950 °C. *Z. Anorg. Allg. Chem.* **1973**, *401*, 172–178.

(41) Tsang, C. F.; Meen, J. K.; Elthon, D. Phase equilibria of the calcium oxide-copper oxide system in oxygen at 1 atm. *J. Am. Ceram. Soc.* **1995**, *78*, 1863–1868.

(42) Suzuki, R. O.; Bohac, P.; Gauckler, L. J. Thermodynamics and phase equilibria in the Ca—Cu—O system. *J. Am. Ceram. Soc.* **1994**, *77*, 41–48.

(43) Chuang, S. Y.; Dennis, J. S.; Hayhurst, A. N.; Scott, S. A. Kinetics of the chemical looping oxidation of H₂ by a co-precipitated mixture of CuO and Al₂O₃. *Chem. Eng. Res. Des.* **2011**, *89*, 1511–1523.

(44) Donat, F.; Hu, W.; Scott, S. A.; Dennis, J. S. Characteristics of copper-based oxygen carriers supported on calcium aluminates for chemical-looping combustion with oxygen uncoupling (CLOU). *3rd International Conference on Chemical Looping*, Gothenburg, Sweden, September 9–11, 2014.

(45) Chuang, S. Y.; Dennis, J. S.; Hayhurst, A. N.; Scott, S. A. Development and performance of Cu-based oxygen carriers for chemical-looping combustion. *Combust. Flame* **2008**, *154*, 109–121.

(46) Singh, V. K.; Ali, M. M.; Mandal, U. K. Formation kinetics of calcium aluminates. *J. Am. Ceram. Soc.* **1990**, *73*, 872–876.

(47) Mohamed, B. M.; Sharp, J. H. Kinetics and mechanism of formation of tricalcium aluminate, Ca₃Al₂O₆. *Thermochim. Acta* **2002**, *388*, 105–114.

(48) Mohamed, B. M.; Sharp, J. H. Kinetics and mechanism of formation of monocalcium aluminate, CaAl₂O₄. *J. Mater. Chem.* **1997**, *7*, 1595–1599.